Journal of Materials Chemistry A

ROYAL SOCIETY OF CHEMISTRY

PAPER

View Article Online
View Journal | View Issue

Cite this: J. Mater. Chem. A, 2022, 10, 24802

Highly efficient bromine capture and storage using N-containing porous organic cages†

Sunggyu Lee, ‡[a] Ilia Kevlishvili, ‡[b] Heather J. Kulik, [b] Hee-Tak Kim, [ad] Yongchul G. Chung *[c] and Dong-Yeun Koh *[ad]

Received 8th July 2022
Accepted 24th October 2022

DOI: 10.1039/d2ta05420e

rsc.li/materials-a

Highly volatile and toxic bromine (Br_2) molecules can be utilized safely in various chemical processes when coupled with efficient separation systems. Herein, we present two different N-containing porous organic cages (POCs), covalent cage 3-R (CC3-R) and formaldehyde tied-reduced covalent cage 3 (FT-RCC3), for vapor Br_2 capture under ambient conditions. They show outstanding sorption capacities (11.02 mmol g^{-1} and 11.64 mmol g^{-1}, respectively) compared with previously reported adsorbents. Reversibility of the Br_2 sorption process has been elucidated experimentally and computationally by identifying bromine species adsorbed at POCs and calculating their binding energies. The strong charge-transfer interactions between adsorbed Br_2 and abundant N atomic sites of the host cages led to the dominant formation of polybromide species (Br_3^- and Br_5^-). Further host–guest interaction between POCs and polybromides determined the reversibility of the Br_2 sorption process—showing partially reversible (>70% recovery) behavior for CC3-R and irreversible (<10% recovery) behavior for FT-RCC3, both of which were affected by the chemical and structural nature of different POCs. DFT calculations further indicate that the formation of carbocationic species (Br_3^- and Br_5^-) and HBr is energetically favorable within the cage, which is in good agreement with the experimental results. This work demonstrates that strong host–guest interactions are essential for highly efficient Br_2 capture and storage performance.

1 Introduction

The diverse reactivity of bromine (Br_2), such as charge compensating anions in cross-coupling reactions and SN_2 reactions, is widely used in industry to produce chemical intermediates and pharmaceuticals. However, the utility of bromine in the chemical industry is largely limited by its severe toxicity, corrosiveness, and volatility, which poses a significant safety concern for the chemical process operation. The high-energy density provided by the bromine redox process in Zn–Br batteries (ZBBs) has been proposed for their low-cost energy storage system (ESS) operation.[1,2] However, the large-scale deployment of the ZBB faces significant hurdles due to the build-up of battery stack pressure, which might induce the leakage of Br_2 into the atmosphere. Toward this end, a small and efficient adsorption-based separation system capable of capturing bromine molecules could accelerate the deployment of the ZBB system. Adsorption-based separation systems provide advantages such as a small device footprint, easy operation, and low-energy usage. Until now, only a few adsorbent materials, such as cobalt- or zirconium-based metal–organic frameworks[3] and vacancy-ordered perovskites,[4] have been investigated for the adsorptive capture of Br_2. New porous adsorbents with high capacity, potential scalability, and chemical stability to Br_2 are highly desirable for capturing Br_2 under ambient conditions, which can contribute to the safe handling of hazardous chemicals.

Halogen compounds, frequently used as electron acceptors, have a good affinity for electron-donating groups. Extensive research into the capture of iodine (I_2) has shown that electron-rich adsorbents would successfully adsorb electron-deficient iodine molecules by forming charge-transfer complexes.[5–7] According to a recent study, ionic functionalized covalent organic frameworks (iCOFs), incorporating abundant binding sites with high electron densities, developed for I_2 capture performed exceptionally well in adsorption capacity and kinetics.[8] The binding sites of iCOFs, including imine, triazine moieties, and cationic sites, would be attributed to their high adsorption capacity by charge-transfer and coulombic interactions with I_2. Br_2 could also preferentially interact with electron-rich species such as imine and triazine. For example,

[a]Department of Chemical and Biomolecular Engineering (BK21 Four), Korea Advanced Institute of Science and Technology, Daejeon, 34141, South Korea. E-mail: dongyeunkoh@kaist.ac.kr

[b]Department of Chemical Engineering, Massachusetts Institute of Technology, Cambridge, Massachusetts, 02139, USA

[c]School of Chemical Engineering, Pusan National University, Busan, 46241, South Korea. E-mail: drygchung@gmail.com

[d]KAIST Institute for NanoCentury, Daejeon, 34141, South Korea

† Electronic supplementary information (ESI) available. See DOI: https://doi.org/10.1039/d2ta05420e

‡ These authors contributed equally.

a computational study shows that Br_2 interacts strongly with the electron-donating nitrogen atom from amine functional groups *via* charge-transfer interaction.[9] Based on these studies, porous adsorbent materials with rich N atoms per volume could be effective for Br_2 capture.

Porous organic cages (POCs) are a new subclass of porous materials with inherent ultramicroporous discrete cages that can be packed together to produce a three-dimensional uniform pore network. POCs have been primarily explored in applications including gas storage,[10a] molecular sensors,[10b] catalyst support,[10c] shape-selective chromatography for aromatic isomer separation,[10d] *etc.* CC3-R, also known as an imine-based POC (Scheme 1a), has shown potential for adsorptive removal of acidic gases[11a] or radioisotope pollutants[11b] due to rich N atoms on the frameworks (14.3% in unit cell atomic composition). Their crystallographic information was also investigated by using single-crystal X-ray diffractometers.[11b] Post-synthetic modifications on CC3-R could further alter the internal cavity size and shape at the atomic level without impacting the chemical composition or crystal packing.[12a] FT-RCC3, a "tied" POC formed by reactions of imine groups in CC3-R with aldehydes (Scheme 1a), has proved to be highly stable in acidic and basic environments.[12b] According to recent research, these POCs can be scaled up using various methods, including batch synthesis,[13a] flow synthesis,[13b] microwave-assisted synthesis,[13c] and twin-screw extrusion.[13d] Herein, we use two distinct N-containing POCs (CC3-R and FT-RCC3) to effectively capture bromine vapor under ambient conditions. CC3-R can be constructed from 1,3,5-triformylbenzene (TFB) and (1R,2R)-cyclohexane-1,2-diamine (CHDA), where the [4 + 6] cyclocondensation reaction of the primary amines and aldehydes results in the formation of the discrete molecular cage through imine linkages (Scheme 1). FT-RCC3 can be readily prepared by reducing the imine group of CC3-R followed by the "tying" method with formaldehyde. Both cages are isostructural as tetrahedral space groups, and their crystal structures formed by window-to-window packing have a three-dimensional diamondoid pore network (Scheme 1b and c). We illustrate the excellent bromine adsorption capacity and kinetics of CC3-R and FT-RCC3 (11.41 mmol g^{-1} and 10.08 mmol g^{-1}, respectively) under static adsorption conditions at room temperature. The drive behind the superior bromine adsorption onto the micropores of the POCs was identified to be the formation of strong charge-transfer complexes either with imine or tertiary

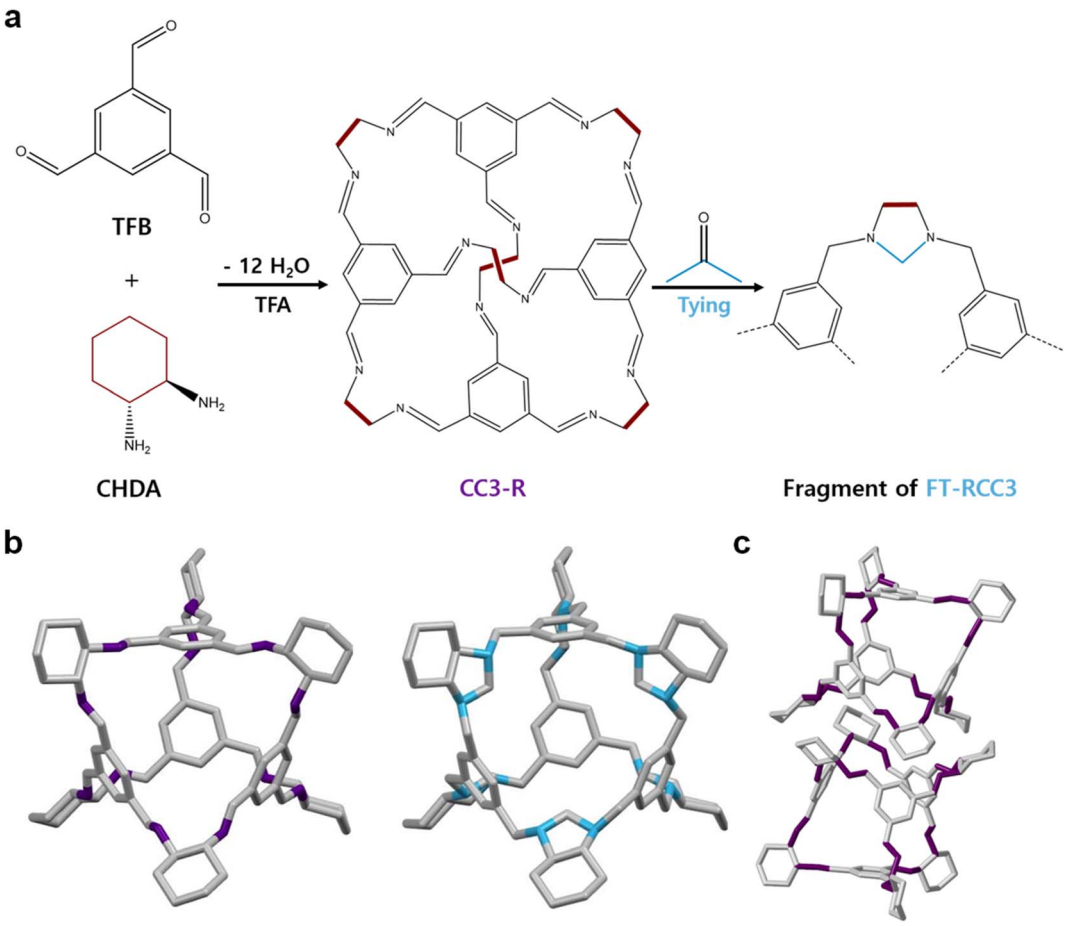

Scheme 1 (a) Synthetic procedure of CC3-R and FT-RCC3. (b) Cage structures of CC3-R (left) and FT-RCC3 (right). Carbons are shown in grey; imine and tertiary amine are shown in purple and light blue; hydrogen atoms are omitted for clarity. (c) Schematic illustration of window-to-window packing in the crystal structure of POCs.

amine sites. DFT calculations elucidated the evolution of polybromide species (Br_3^- and Br_5^-) when bromine vapors are adsorbed and stabilized in the POCs. The degree of the stability offered by distinct N-groups determined the reversibility of the Br_2 capture process utilizing POCs.

2 Experimental

2.1 Materials and methods

2.1.1 Materials. All starting materials and solvents were obtained from commercial sources and used without further purification. Anhydrous dichloromethane (DCM, >99%), 1,3,5-triformylbenzene (TFB, 98%), and potassium iodide (KI, 99.5%) were purchased from TCI. Trifluoroacetic acid (TFA, 99%), (1R,2R)-cyclohexane-1,2-diamine (CHDA, 98%), sodium thiosulfate pentahydrate (99.5%), and paraformaldehyde (96%) were purchased from Alfa Aesar.

2.1.2 Preparation of porous organic cages (POCs). CC3-R and FT-RCC3 were prepared as previously reported in their homochiral form.[12b,14] The detailed synthetic procedures are described in the ESI.†

2.1.3 Static bromine vapor capture. The static bromine vapor capture was conducted using the customized system,[3a] shown as a photograph in Fig. S4.† ~250 mg of activated POCs were loaded in a glass tube that was connected (*via* a U-shaped glass adapter) to another tube equipped with a Teflon valve. The empty glass tube was filled with liquid Br_2 and tightly closed with the Teflon valve. The system was then evacuated and kept under static vacuum. The Teflon valve sealing the bromine-containing tube was then opened letting the bromine vapors fill the POC-containing tube. The POC was exposed to bromine vapors for certain times, after which the bromine-containing tube was again sealed by the screw-cap. Excess bromine was then removed under vacuum.

2.1.4 Measurement of bromine uptake capacity. The bromine uptake capacity was measured using two kinds of methods; the weight increment of the POCs and iodometric titration method. The static bromine vapor uptake capacity (q_t, mmol g^{-1}) at certain time was calculated with the following eqn (1):

$$q_t = \frac{(m_t - m_0) \Big/ M_{w_{Br_2}}}{m_0}, \quad (1)$$

where q_t (mmol g^{-1}) denotes the static bromine vapor capture capacity at time t, m_t (g) denotes the weight of the glass tube containing POCs at time t, m_0 (g) denotes the weight of the glass tube containing POCs before adsorption, and $M_{w,Br2}$ (g mol^{-1}) denotes the molecular weight of bromine. The measurement of bromine uptake capacity using the gravimetric method was repeated 2–3 times at each adsorption time point.

The experimental procedure of the titration method was performed as previously reported.[3a] For the measurement of bromine uptake capacity using the titration method, captured bromine was desorbed and trapped in the storage flask. The glass tube containing Br_2@POC was connected to a storage flask equipped with a Teflon screw-cap. Before the desorption procedure, the system was evacuated and kept under static vacuum. The glass tube containing Br_2@POC was enclosed by heating wire controlled by a heat controller, while the storage flask was immersed in a Dewar flask filled with liquid N_2. The temperature of the heating wire was then gradually raised from room temperature to 200 °C and kept at 200 °C for 8 hours under dynamic vacuum conditions. Evolved Br_2 was trapped in the cooled storage flask. At the end of time, the storage flask was tightly sealed and allowed to warm up to room temperature. The amounts of trapped Br_2 were determined by iodometric titration. A short glass tube was connected to the outlet joint of the storage flask. The resulting space (joint + the tube) was filled with an aqueous solution of KI (10% w/v). The Teflon cap was then quickly opened and closed, sucking some of the solution into the bromine-containing flask. The resulting solution was then titrated with 0.2 M aqueous solution of $Na_2S_2O_3$ (2 eq. of $Na_2S_2O_3$ for 1 eq. of Br_2). Soluble starch indicator (obtained by boiling 0.1 g of starch in 20 mL of water) was added towards the end of the titration, to allow easier determination of the titration end point.

2.2 Characterization methods

Attenuated total reflectance Fourier-transform infrared spectra were collected by using a Nicolet iS50, spectrometer in transmittance mode. The wavenumber range was set from 500 cm^{-1} to 4000 cm^{-1} with a resolution of 4 cm^{-1}. High-resolution SEM imaging of POC crystal structures was achieved by using an FEI Magellan™ 400. Powder X-ray diffraction (PXRD) patterns were measured on a RIGAKU SmartLab X-ray diffractometer with Cu Kα radiation ($\lambda = 1.5406$ Å) in the 2-theta range of 5°–40° with a step of 0.2°. Liquid ^{1}H NMR spectra in $CDCl_3$ were recorded at 600 MHz. Solid-state ^{13}C CPMAS NMR spectra were recorded at 150.95 MHz at a spinning rate of 30 kHz. ^{13}C CPMAS NMR conditions for the ^{1}H–^{13}C polarization experiment used a π/2 pulse of 2.5 μs, contact time of 2 ms, delay time of 5 s, and 1024 scans. Chemical shifts were referenced to a solid shift at 38.95 ppm relative to TMS. All NMR spectra were collected by using a Bruker Avance Neo 600 spectrometer. X-ray photoelectron spectroscopy (XPS) spectra were collected using a Sigma Probe spectrometer, equipped with a monochromatic Al Kα X-ray source ($h\nu = 1486.7$ eV) at ultra-high vacuum. Nitrogen (N_2) sorption isotherms at 77 K were measured by a volumetric method using a Micromeritics ASAP 2020 gas sorption analyzer. Brunauer–Emmett–Teller (BET) areas were calculated from N_2 isotherms collected at 77 K. Evolved gas analysis (EGA) was performed using a NETZSCH STA-GC-MS under an ultra-high purity (UHP) argon flow. The samples were heated up from 80 °C to 800 °C with a heating rate of 10 °C min^{-1}. Raman spectra were recorded using a LabRAM HR evolution visible_NIR Raman spectrometer with a 514 nm laser. Elemental compositions were measured by using a ZSX Primus II X-ray fluorescence spectrometer (XRF) and FlashEA 1112 elemental analyzer (EA).

3 Results and discussion

3.1 Structural characterization of CC3-R and FT-RCC3

Powder X-ray diffraction (PXRD) and scanning electron microscopy (SEM) were used to check the structural integrity of

the POCs as they were synthesized. Both N-containing POCs were highly crystalline, as indicated by PXRD, and these patterns were in good agreement with the simulated structure (Fig. 1a and b). POC crystals had highly ordered octahedral structures assembled by window-to-window packing, as seen in SEM images (Fig. 1c and d), and this packing was unaffected by the formaldehyde post-synthetic modification. To further verify the successful synthesis and transformation of POCs, we carried out additional analyses, including Fourier-transform infrared spectroscopy (FT-IR), $^{1}H/^{13}C$ nuclear magnetic resonance (NMR) spectroscopy, and X-ray photoelectron spectroscopy (XPS). FT-IR spectra showed a characteristic –C═N– stretching band (1643 cm^{-1}) derived from the imine linkage of CC3-R without the appearance of a characteristic band of amino groups (3342 cm^{-1}) and aldehyde groups (1690 cm^{-1}) from CHDA and TFB (Fig. 1e and S1†). These findings demonstrated that TFB and CHDA had undergone a complete Schiff-base reaction. Meanwhile, an additional characteristic aliphatic C–H stretching band at 2794 cm^{-1} and the disappearance of the –C═N– stretching band (1643 cm^{-1}) in the FT-IR spectrum of

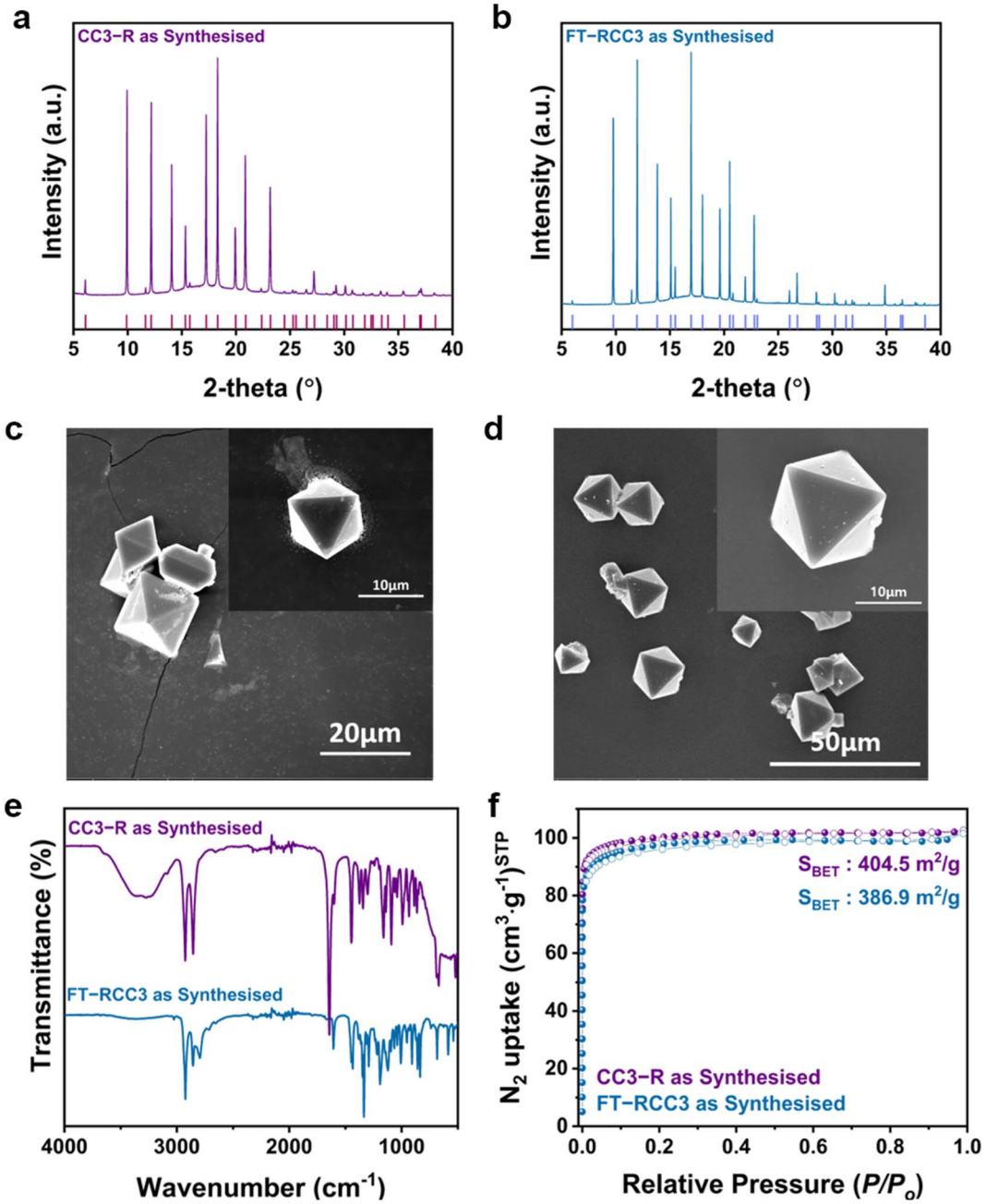

Fig. 1 Structural characterization of CC3-R and FT-RCC3. PXRD patterns of (a) CC3-R and (b) FT-RCC3. Simulated peaks are shown as below tick marks. SEM images of (c) CC3-R and (d) FT-RCC3. Inset images represent the high-resolution images. (e) FT-IR spectra of CC3-R and FT-RCC3. (f) N_2 sorption isotherms of CC3-R and FT-RCC3.

FT-RCC3 indicated that formaldehyde had been successfully connected with the parent imine cage *via* post-synthetic modification. Solid-state ^{13}C cross-polarization magic angle spinning (CPMAS) NMR and XPS spectra further confirmed this result, which showed an additional aliphatic signal at 79.3 ppm associated with "tied" groups (–NCH_2N–) and the binding energy of tertiary amine at 398.40 eV and 399.09 eV (Fig. S2 and S3†). Additionally, the textural properties of the as-synthesized POCs were analyzed with the N_2 physisorption at 77 K. Both POCs showed type I N_2 physisorption isotherms at 77 K, indicating their inherent ultramicroporous structures (Fig. 1f and Table S1†). FT-RCC3 had a lower Brunauer–Emmett–Teller (BET) specific surface area and lower total pore volume than CC3-R due to the tying of the internal cavity.

3.2 Static Br_2 adsorption performance of CC3-R and FT-RCC3

We measured the vapor Br_2 adsorption capacities and uptake curves of N-containing POCs (CC3-R and FT-RCC3) under ambient, static conditions (25 °C and 0.3 bar of Br_2 vapor pressure). The experimental setup is shown in Fig. S4.† Based on the gravimetric measurements, CC3-R and FT-RCC3 exhibited high Br_2 adsorption capacities of 9.49 and 9.71 mmol g^{-1} in the first 24 hours of adsorption, respectively; 11.02 mmol g^{-1} and 11.64 mmol g^{-1} in the first 48 hours of adsorption, respectively (Fig. 2a and b). They outperformed the Br_2 adsorption capacity (4–70 times) of previously reported adsorbents[3a,15] (Table S1†). The high capture performance would be attributed to their large number of N atoms per discrete molecular cage (14.3% of unit cell atomic composition). Additionally, these values are higher when compared to calculated adsorption capacities from the GCMC simulation[25] (Table S9†). As the molecular simulation snapshots (Fig. S34†) indicated, a single Br_2 is adsorbed inside each cage while the channels connecting the cages are occupied by a single Br_2 molecule. The discrepancy between the simulated and experimental saturation uptake is likely a combination of the formation of polybromide species (further discussed in the following sections) and the expansion of the cage-to-cage channel distance, which could contribute to the additional adsorption sites for Br_2 molecules. Notably, FT-RCC3 showed faster adsorption kinetics than CC3-R. These findings suggest that tertiary amine groups interact with bromine molecules more favorably than imine groups, which is in line with earlier research;[9a] additionally, the equilibrium sorption capacities were affected by the total pore volume and BET surface area of these materials (Table S1†). Furthermore, the adsorption kinetic curves of both POCs (Fig. 2 and S5†) were well matched with a pseudo-second-order adsorption model (R-square values of CC3-R and FT-RCC3 are 0.9920 and 0.9905, respectively), showing that the adsorption rate is regulated by a chemical reaction between bromine molecules and POC frameworks.[16] Interestingly, the variations in uptake capacities evaluated by two different methods (gravimetric *versus* titration) were greater in FT-RCC3 than in CC3-R, indicating stronger irreversible chemisorption occurring in FT-RCC3 (Fig. 2c). The titration was performed using the collected Br_2 after the thermal desorption of the bromine from the POCs, and the adsorption capacity calculated from the gravimetric method was higher than that of the titration method due to the existence of a small portion of the condensed Br_2 phase. CC3-R with abundant imine sites showed partially reversible sorption of Br_2 with the recovery of Br_2 by thermal desorption (>100–200 °C) observed up to 70% while FT-RCC3 with sterically hindered tertiary amine sites showed almost irreversible chemisorption—Br_2 recovery was only up to 10%. After thermal desorption of Br_2 from both POCs, halogen compounds such as ionized bromine atoms ($^{79}Br^+$, $^{81}Br^+$) and hydrogen bromide ions ($^1H^{79}Br^+$, $^1H^{81}Br^+$) were identified by coupling the evolved gas analyzer with a mass spectrometer (Fig. S6 and S7†). The time–intensity curve (TIC) tailing was longer in FT-RCC3 with significantly delayed desorption behavior, implying the increased number of residual bromine compounds trapped in FT-RCC3. For FT-RCC3, a considerable fraction of the Br_2 remained within the interior cavity and would not be desorbed by heat treatment due to a strong interaction with host cages, resulting in almost irreversible chemisorption.

The PXRD patterns of CC3-R and FT-RCC3 after sorption–desorption measurement of Br_2 have confirmed that POCs lost their crystal packing (Fig. S8†), most likely due to the preferential desorption of Br_2 that are weakly attached to the cage surface or interstitial spaces between the cages. Additionally, the integrity of the cage structure after Br_2 adsorption was confirmed by solid-state ^{13}C CPMAS NMR, X-ray fluorescence spectroscopy, and elemental analysis (Fig. S9, Tables S3 and S4†). NMR spectra of both POCs showed broad signals after Br_2 adsorption, demonstrating that the captured bromine molecules impacted the mobility and chemical environment of carbon atoms.[11a] The new peaks at 50.97 ppm and 54.98 ppm correspond to the changes in the electromagnetic field in carbon atoms attached to N atoms due to the strong adsorption of Br_2 onto the N atoms, while primary aliphatic (24.97 ppm and 30.99 ppm) and aromatic (140.71 ppm) carbon structures remained unchanged. These results indicated that discrete molecular cages are modified by the interactions with bromine molecules, resulting in the changes in structural and magnetic properties without decomposition (or destruction) of the parent unit cage structures.[17] After thermal treatment, the atomic compositions of "physical mixture of monomers," which mimics the situation when the cage fragments are formed after desorption, were changed (Table S3†); C/N and C/H ratios were increased after thermal treatment. In contrast, the elemental compositions of POCs after the bromine sorption–desorption cycle exhibited similar C/N and C/H ratios to those of pure POCs, indicating that the unit cage frameworks are nearly intact. We also confirmed that the Br/C ratio decreased after the thermal desorption procedure (Table S4†), indicating that bromine molecules were released while the carbon composition of the cage framework was almost maintained. We determined that the Raman spectra of POCs after Br_2 sorption–desorption were unchanged compared to those of pure POCs, only appearance of characteristic bands of charge-transfer complexes (Fig. S10 and S11†), while they differed from

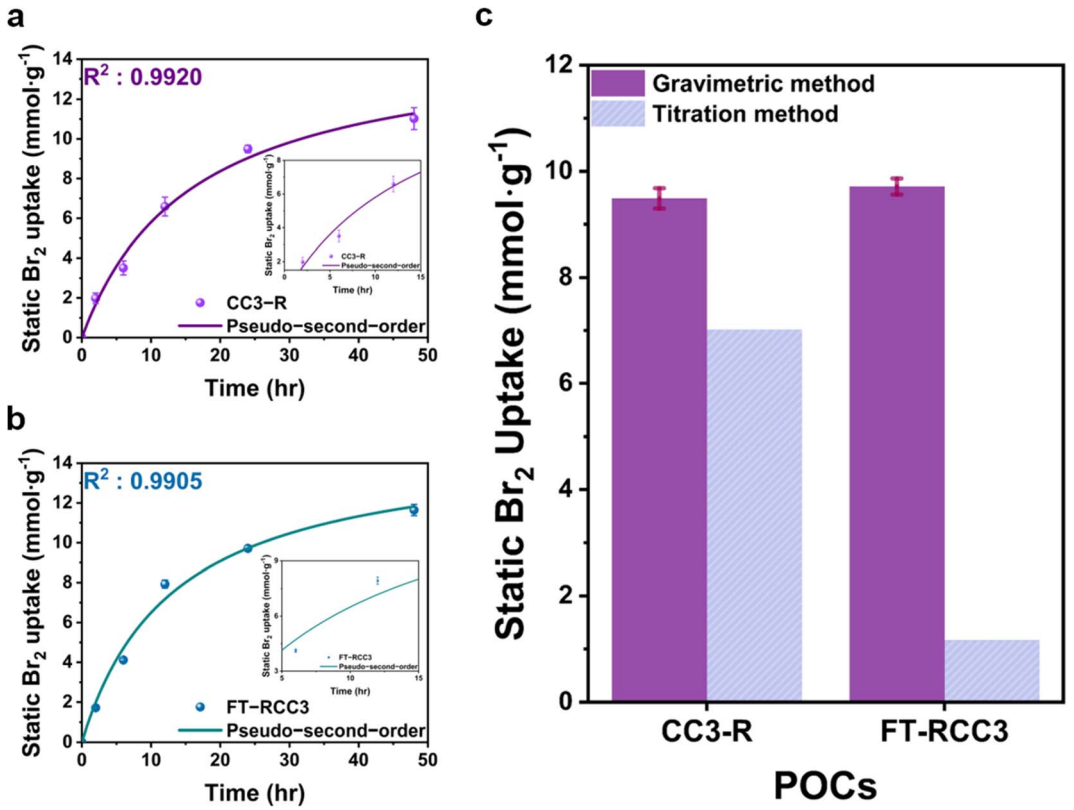

Fig. 2 Static Br_2 adsorption performance. Gravimetric measurement of static Br_2 vapor uptake capacities of (a) CC3-R and (b) FT-RCC3 as a function of time at 25 °C and near ambient pressure. (c) Comparison of static Br_2 capture capacities over 24 hours based on the measurement methods. The error bar represents the variation in Br_2 uptake with 2–3 replicate experiments at each adsorption time point. Inset images are the magnification parts of multiple adsorption points for verifying the error bars.

monomers (Fig. S12†); the characteristic bands of TFB (~1596 cm^{-1} and 1688 cm^{-1}) have not appeared in the Raman spectra of Br_2@CC3-R. Additionally, we demonstrated that two POCs retained their adsorption capabilities over 5 cycles of bromine sorption–desorption procedures (Fig. S13†). Overall, these findings revealed that trapped bromine only disrupted the regular packing of POCs, without unit cage destruction and decrease in their adsorption capabilities.

3.3 Br_2 adsorption mechanism

To support our hypothesis, we used several analyses to describe the adsorbents as synthesized (denoted as CC3-R and FT-RCC3, respectively) and after bromine capture (denoted as Br_2@CC3-R and Br_2@FT-RCC3, respectively). Time-resolved FT-IR spectra showed that during Br_2 adsorption, Br_2@CC3-R exhibited reduced intensities of the –C═N– bond at 1643 cm^{-1}, C–N bond at 1160 cm^{-1}, and C–H bond bands at 1445 and 990 cm^{-1}; additionally, the peak associated with the C═C bond at 1600 cm^{-1} underwent a gradual redshift[8,13c,18] (Fig. 3a). Some new vibration bands emerged at 647 cm^{-1} and in the range of 1668–1698 cm^{-1}, representing C–Br and N–Br interactions, respectively. In the high wavenumber range, gradual peak broadening was observed in the 2300–3200 cm^{-1} region with increasing adsorption time, indicating intermolecular interaction among cyclohexane rings on the POC framework and adsorbate molecules[19] (Fig. S14†). These spectral changes indicate that the functional groups of CC3-R including imine, cyclohexane, and phenyl rings all contributed to the formation of charge-transfer complexes with bromine molecules.[8] For Br_2@FT-RCC3, similar results showed that all functional groups interacted with bromine molecules (Fig. 3b and S15†). The new vibration bands appeared at 507 cm^{-1} and 1694 cm^{-1}, representing C–Br and N–Br bonds, respectively. The peak assigned to the C═C bond at 1607 cm^{-1} underwent a gradual redshift, also suggesting the existence of charge-transfer interactions between host cages and guest bromine molecules in FT-RCC3.

X-ray photoelectron spectroscopy (XPS) was used to precisely measure the atomic states of the trapped bromine species. The Br_{3d} spectra revealed the two major component peaks, which were attributed to the physisorbed bromine species including Br_2 molecules and bromine derivatives such as Br^- and HBr (68.9 eV and 70.4 eV) and bromine molecules adsorbed with host cages as charge-transfer complexes[20] (67.8 eV) (Fig. 4a). These findings were further supported by the Br_{3p} spectra, showing the characteristic peak of charge-transfer complexes (181.1 eV and 187.2 eV) (Fig. S16†). Furthermore, the adsorption of Br_2 at CC3-R caused a blue shift from 398.10 eV to 398.45 eV in the N_{1s} spectra (Fig. 4b), suggesting that all N atoms in the cage interacted with Br_2.[8] The new peak at 400.78 eV is associated with the N–Br bond[21] of the charge-transfer complexes

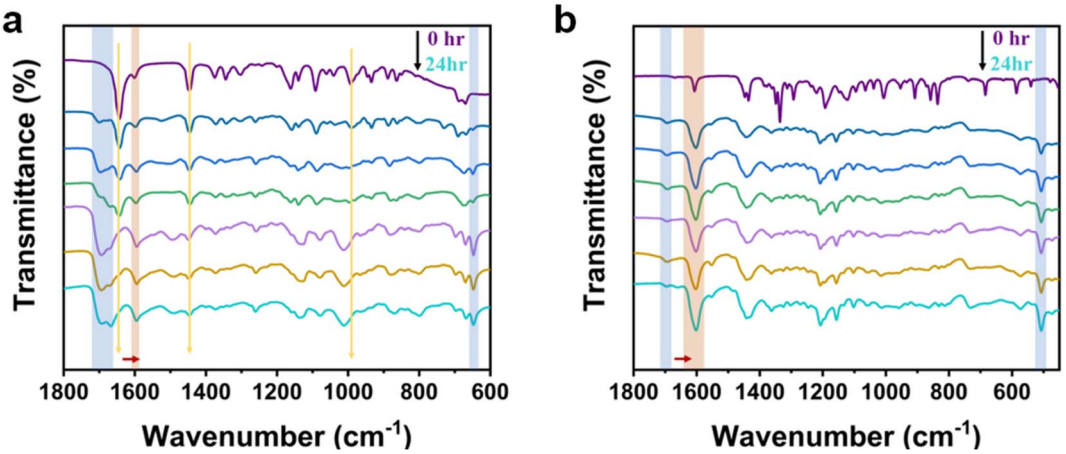

Fig. 3 FT-IR spectra of (a) CC3-R and (b) FT-RCC3 during static Br_2 adsorption at 25 °C.

between the imine linkage of CC3-R and Br_2. The C_{1s} spectra (Fig. S17†) also showed a peak shift from 284.24 eV to 284.35 eV, indicating its interaction with bromine, which was consistent with previous FT-IR results (Fig. 3a). In the case of FT-RCC3, similar findings were obtained in all of the XPS elements (Fig. 4c, S16 and S17†). The Br_{3d} spectra also showed the peaks of two major components, including physisorbed bromine species (68.5 eV and 70.0 eV) and bromine adsorbed as charge-transfer complexes (67.4 eV). The N_{1s} and C_{1s} XPS spectra of Br_2@FT-RCC3 revealed peak shifts of all N_{1s} and C_{1s} peaks, indicating their strong interactions with bromine molecules. These results clearly demonstrated that the trapped bromine

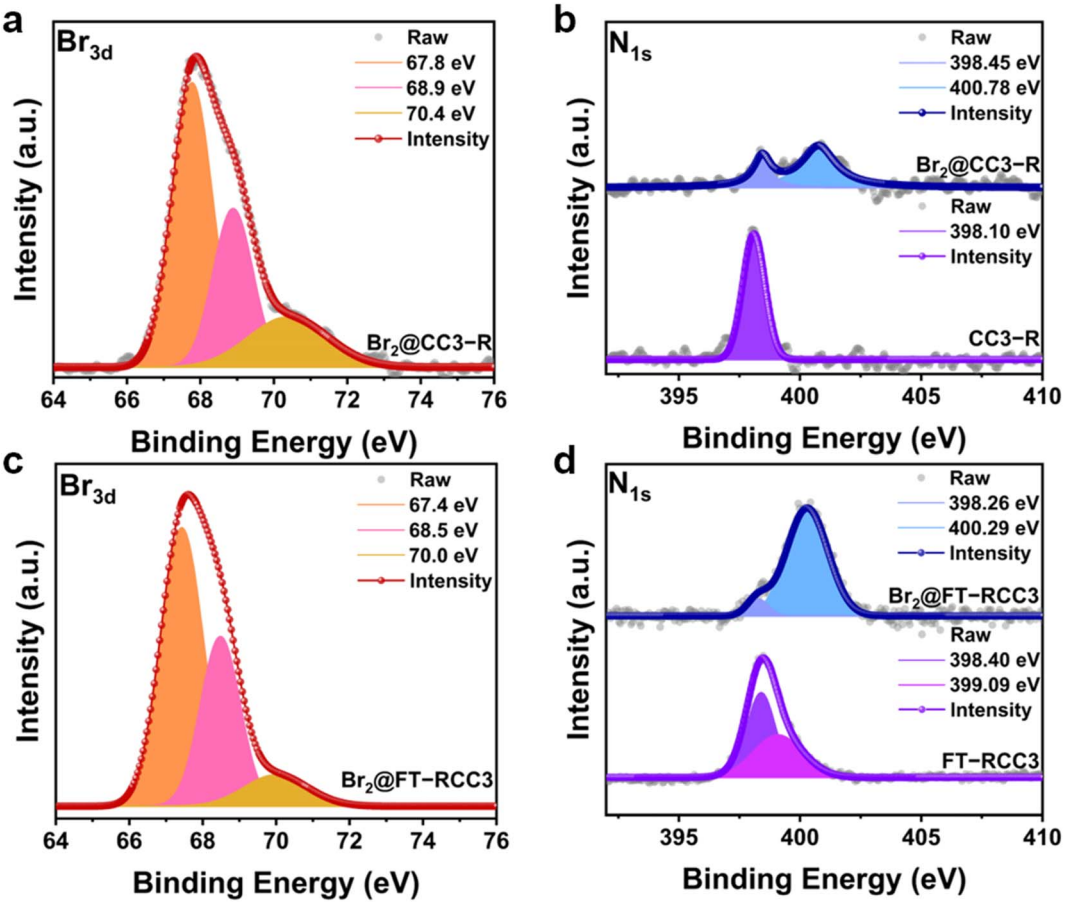

Fig. 4 XPS spectra of bromine-captured POCs. Br_{3d} XPS spectra of (a) Br_2@CC3-R and (c) Br_2@FT-RCC3. N_{1s} XPS spectra of (b) pristine CC3-R and Br_2@CC3-R and (d) pristine FT-RCC3 and Br_2@FT-RCC3. Br_2-captured POCs are prepared under static conditions at 25 °C and near ambient pressure and are denoted as Br_2@CC3-R and Br_2@FT-RCC3, respectively.

molecules interacted with host cages, particularly at the N atomic sites, forming charge-transfer complexes.

We further employed Raman spectroscopy to identify adsorbed bromine species (Fig. 5ab, and S18†). Unlike pure Br_2 vapor represented by the single Raman band at 323 cm^{-1},[22] Br_2@CC3-R showed four bands at 161 cm^{-1}, 212 cm^{-1}, 251 cm^{-1}, and 270 cm^{-1}. These bands are associated with symmetric stretching vibration of polybromide Br_3^- (161 cm^{-1}), asymmetric stretching vibration of polybromide Br_3^- and Br_5^- (212 cm^{-1}), symmetric stretching vibration of polybromide Br_5^- and Br_2 molecules which have confinement effect (251 cm^{-1}), and symmetric stretching vibration of concerted Br_2 molecules (270 cm^{-1}),[23] respectively. Similarly, Br_2@FT-RCC3 presented two bands that showed high intensity at 160 cm^{-1} and 202 cm^{-1}, associated with symmetric stretching vibration of polybromide Br_3^-, asymmetric stretching vibration of polybromide Br_3^-,[24] and the other two bands, which exhibited relatively low intensity at 234 cm^{-1} and 302 cm^{-1}, associated with symmetric stretching vibration of the intercalated Br_2 molecule, and symmetric stretching vibration of the Br_2 molecule in the condensed phase,[23b,24] respectively. These findings demonstrated that bromine molecules could exist in porous organic cages as both polybromide species (Br_3^- and Br_5^-) and pure bromine molecules; specifically, polybromide species dominated. Notably, the characteristic band of Br_5^- was only identified in CC3-R, indicating that the formation of Br_5^- in FT-RCC3 would be unfavorable due to the steric hindrance effect caused by the tied-methylene group. It is also worth noting that Br_3^- with FT-RCC3 has larger adsorption energy than Br_3^- and Br_5^- with CC3-R (Table S5†), which means that the polybromide species in CC3-R could be desorbed more easily, resulting in better reversibility than FT-RCC3.

3.4 Computational studies of Br_2 adsorbed POCs

Additionally, we computed the vibrational frequencies of isolated Br_n (n = 2, 3, 4, and 5) molecules as they were adsorbed inside the POC to support our experimental Raman results (detailed computational methods are discussed in the ESI†). The calculated Raman bands at 285 cm^{-1} and 270 cm^{-1} were observed in the case of adsorbed two Br_2 and three Br_2 molecules, respectively, for the CC3 cage (Fig. S28 and S29†). These Raman bands correspond to the experimentally observed Raman bands for CC3 (~251 cm^{-1} and 270 cm^{-1}). Since the simulated Raman peaks typically redshift to 10–20 cm^{-1} (see Table S7†), it is reasonable to conclude that the experimentally observed Raman peaks correspond to the concerted vibration of Br_2 molecules within the cage. However, we were not able to resolve the origin of the largest intensity peak (~160 cm^{-1}) observed in the experiments. Since our calculations involve a single cage, we speculate that these peaks originate from the Br_2 molecules that are adsorbed between the cages, indicating that the formation of polybromide species is mainly affected by the presence of intermolecular pores of POCs. It was also reported that the vibration frequency of the Br–Br bond, ω_{Br-Br}, was strongly affected by the external environment and charge density state (*e.g.*, intermolecular interaction between bromine chains and that between chains and host cages).[23] In this regard, as the number of molecules in the cage increased, the bromine molecule would have a highly confined effect, resulting in a redshift of its Raman band. These calculated vibrational frequencies were in good agreement with our experimental Raman bands and previous studies.[23,24]

To better understand of the mechanism of charge-transfer complex formation and physicochemical states of bromine species, DFT calculations were carried out to compute the binding and formation energies as a function of bromine species and the number of unreacted bromine molecules within the two cages. The calculated adsorption energy between CC3-R and Br_3^- is 33.9 kcal mol^{-1}, and the binding energy between FT-RCC3 and Br_3^- is 74.0 kcal mol^{-1}, respectively (Fig. 6 and Table S5†). The differences in the adsorption energies of both POCs indicate the difficulty of desorbing the adsorbed bromine species in CC3-R and FT-RCC3, which is likely the culprit of the irreversible desorption of bromine species from FT-RCC3. The binding energy of the first bromine molecule is more favorable with FT-RCC3 when compared to CC3-R, which is primarily facilitated through stronger electrostatic interactions (Table S6†). These calculation results provide a reasonable explanation

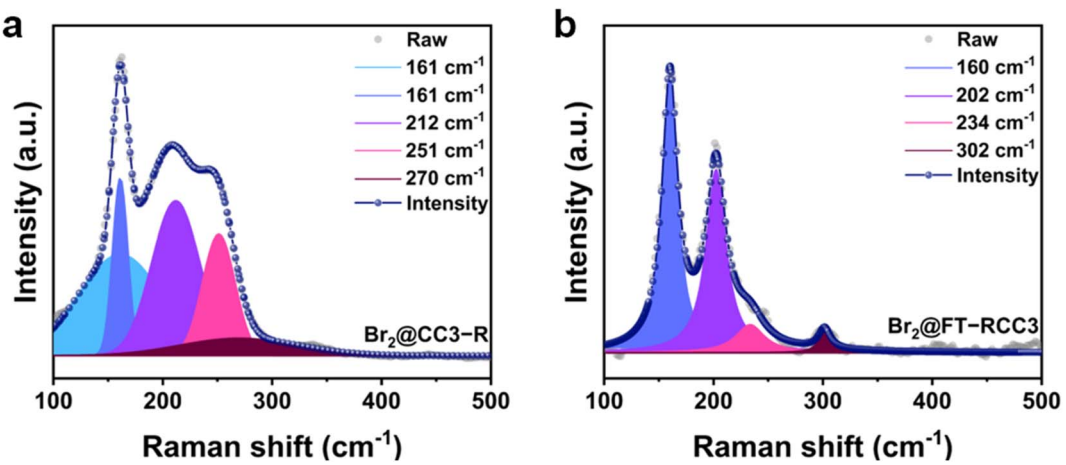

Fig. 5 Raman spectra of (a) Br_2@CC3-R and (b) Br_2@FT-RCC3.

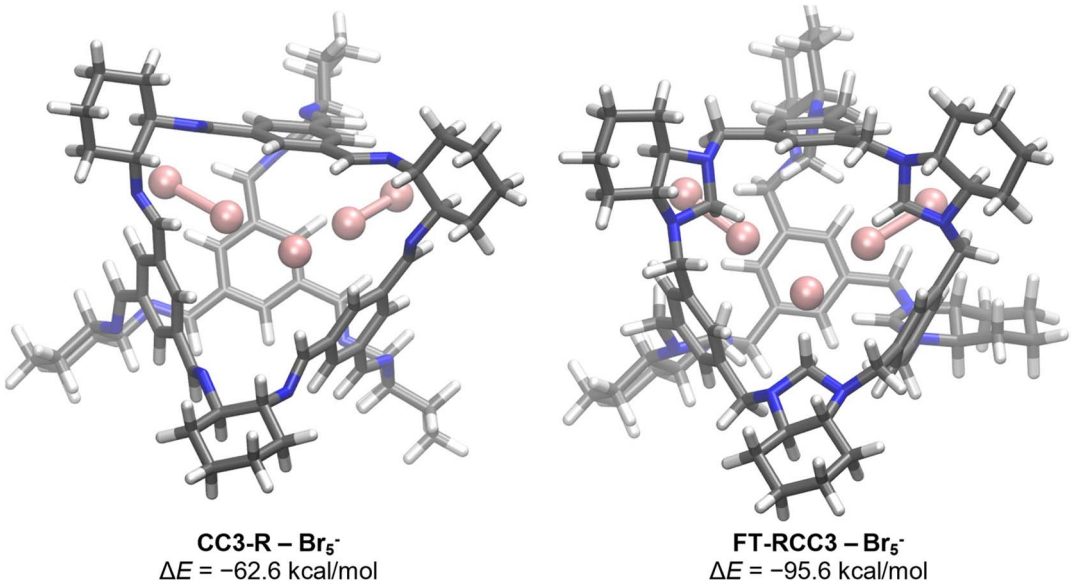

Fig. 6 Optimized structures of CC3-R and FT-RCC3 with adsorbed polybromide Br_5^-. All energies are relative to free POCs and 3 bromine molecules.

for the faster Br_2 uptake kinetics of FT-RCC3 than CC3-R at lower adsorption time (<12 hours). However, the binding of additional bromine molecules is more favored with CC3-R, which can form strong halogen bonding interactions with imine nitrogen, increasing charge-transfer interactions (Fig. S31†), and leading to a short N···Br interatomic distance (Fig. S33A†). On the other hand, FT-RCC3 is primarily stabilized through additional C–H···Br through-space interactions. These are facilitated through two distinct orbital interactions. First, lone pair-σ* interactions between the tertiary amine and bromine molecules are still present with FT-RCC3 but occur through hyperconjugation of the nitrogen lone pair to the energetically less favorable C–H σ* orbital due to diminished orbital overlap (Fig. S32†). Additional charge-transfer interactions between the bromine lone pair (lp) and "tying" C–H σ* are also present which is unique to FT-RCC3 and leads to additional stabilization. These factors together lead to a longer N···Br interatomic distance and a shorter H···Br interatomic distance. Furthermore, due to the presence of lp → σ* interactions, there is a significant elongation of the "tying" C–H bond (Fig. S33B†), which can promote the deprotonation and HBr formation with FT-RCC3. Therefore, FT-RCC3 can form significantly more stable polybromide species, through more favorable deprotonation of the "tying" methylene group (Fig. S30†). We hypothesized that the tied-methylene groups in FT-RCC3 decrease the mobility of trapped bromine species in the host cages, resulting in more stable storage of bromine in polybromide species forms that are not easily desorbed. For CC3-R, bromine species can move more freely in the cage structure compared to FT-RCC3. DFT calculation results provide additional support for this hypothesis. We found that the calculated formation energy of carbocation species (Br_3^- and Br_5^-) is significantly more exergonic for FT-RCC3 than it is for CC3-R. Based on these calculations, we conclude that HBr and Br_5^- species are the most energetically stable species compared with other bromine species. This is consistent with experimental Raman spectra analyses that bromine molecules would mainly exist as polybromide states (Fig. 5a and b), and EGA-MS analysis showed that the hydrogen bromide was detected at both POCs after the thermal treatment process (Fig. S6 and S7†).

4 Conclusion

In this work, we present the new application of porous organic cages as potential candidates for highly toxic and volatile Br_2 vapor capture. For efficient bromine capture, several factors should be considered including textural properties, affinity with bromine molecules, and densities of binding sites. Two different N-containing POCs (CC3-R and FT-RCC3), which have high porosity and many favorable binding sites for Br_2, show high Br_2 vapor capture performance under static conditions. FT-RCC3, which has a lower total pore volume, exhibits a faster bromine adsorption kinetics than CC3-R with similar adsorption capacities, indicating that the affinity between host materials and guest molecules is the critical factor for enhancing capture performance. Interestingly, both POCs showed different desorption abilities owing to their structural difference. DFT calculation results show that the formation of carbocationic species (Br_3^- and Br_5^-) and HBr is energetically more favorable within the cage. The energy decomposition analyses showed that both POCs showed highly stabilized halogen bonding interaction with bromine. This study demonstrates the essential role of strong host–guest interaction in the development of highly efficient capture and storage performance adsorbents. We believe that these N-containing POCs, coupled with their good processability and synthetic scalability, can be utilized for toxic and volatile halogen vapor capture.

Author contributions

All authors have approved the final version of the manuscript.

Conflicts of interest

The authors declare no competing financial interest.

Acknowledgements

This work was supported by the "2021 Joint Research Project of Institutes of Science and Technology" and the National Research Foundation of Korea (NRF) funded by the Ministry of Science and ICT, South Korea (NRF-2021R1C1C1012014). This work was also supported by the Industrial Technology Alchemist Project (e-Biorefinery: integration of direct air capture, C1 conversion, and synthetic biology, 20019268) funded by the Ministry of Trade, Industry & Energy (MOTIE, Korea). This work was partially supported (to H. J. K. and I. K.) by the NSF Center for the Chemistry of Molecularly Optimized Networks (MONET), CHE-2116298. This work was partly supported by the National Research Foundation of Korea (NRF) for financial support from a grant funded by the Korea government (MSIT) (No. 2020R1C1C1010373).

References

1 G. L. Soloveichik, Metal-free energy storage, *Nature*, 2014, **505**, 163–165.

2 C. Wang, Q. Lai, K. Feng, P. Xu, X. Li and H. Zhang, From zeolite-type metal organic framework to porous nano-sheet carbon: High activity positive electrode material for bromine-based flow batteries, *Nano Energy*, 2018, **44**, 240–247.

3 (*a*) Y. Tulchinsky, C. H. Hendon, K. A. Lomachenko, E. Borfecchia, B. C. Melot, M. R. Hudson, J. D. Tarver, M. D. Korzyński, A. W. Stubbs, J. J. Kagan, C. Lamberti, C. M. Brown and M. Dincă, Reversible Capture and Release of Cl_2 and Br_2 with a Redox-Active Metal-Organic Framework, *J. Am. Chem. Soc.*, 2017, **139**, 5992–5997; (*b*) J. Pang, S. Yuan, D. Du, C. Lollar, L. Zhang, M. Wu, D. Yuan, H.-C. Zhou and M. Hong, Flexible Zirconium MOFs as Bromine Nanocontainers for Bromination Reactions under Ambient Conditions, *Angew. Chem.*, 2017, **129**, 14814–14818.

4 (*a*) Y.-P. Lin, B. Xia, S. Hu, Y. Zhong, Y.-E. Huang, Z.-Z. Zhang, N. Wu, Y.-W. Wu, X.-H. Wu, X.-Y. Huang, Z. Xiao and K.-Z. Du, Reversible Release and Fixation of Bromine in Vacancy-Ordered Bromide Perovskites, *Energy Environ. Mater.*, 2020, **3**, 535–540; (*b*) Y.-P. Lin, X.-Y. Huang and K.-Z. Du, Br_2-free method for XBr_3 (X= Cs, $C_8H_{20}N$, $C_{16}H_{36}N$) synthesis: Br_2 solid storage and separation from aqueous solution, *Mater. Chem. Phys.*, 2022, **280**, 125820.

5 L. He, L. Chen, X. Dong, S. Zhang, M. Zhang, X. Dai, X. Liu, P. Lin, K. Li, C. Chen, T. Pan, F. Ma, J. Chen, M. Yuan, Y. Zhang, L. Chen, R. Zhou, Y. Han, Z. Chai and S. Wang, *Chem*, 2021, **7**, 699–714.

6 C. Wang, Y. Wang, R. Ge, X. Song, X. Xing, Q. Jiang, H. Lu, C. Hao, X. Guo, Y. Gao and D. Jiang, A nitrogen-rich covalent organic framework for simultaneous dynamic capture of iodine and methyl iodide, *Chemistry*, 2018, **24**, 585–589.

7 (*a*) M. Xu, T. Wang, L. Zhou and D. Hua, Fluorescent conjugated mesoporous polymers with N,N-diethylpropylamine for the efficient capture and real-time detection of volatile iodine, *J. Mater. Chem. A*, 2020, **8**, 1966–1974; (*b*) T.-H. Niu, C.-C. Feng, C. Yao, W.-Y. Yang and Y.-H. Xu, Bismidazole-based conjugated polymers for excellent iodine capture, *ACS Appl. Polym. Mater.*, 2021, **3**, 354–361.

8 Y. Xie, T. Pan, Q. Lei, C. Chen, X. Dong, Y. Yuan, J. Shen, Y. Cai, C. Zhou, I. Pinnau and Y. Han, Ionic Functionalization of Multivariate Covalent Organic Frameworks to Achieve an Exceptionally High Iodine-Capture Capacity, *Angew. Chem. Int., Ed. Engl.*, 2021, **60**, 22432–22440.

9 (*a*) S. Salai Cheettu Ammal, S. P. Ananthavel, P. Venuvanalingam and M. S. Hegde*, UVPES and ab Initio Molecular Orbital Studies on the Electron Donor-Acceptor Complexes of Bromine with Methylamines, *J. Phys. Chem. A*, 1997, **101**, 1155–1159; (*b*) M. M. Naseer, A. Bauzá, H. Alnasr, K. Jurkschat and A. Frontera, Lone pair-π vs σ hole-π interactions in bromine head-containing oxacalix[2]arene[2]triazines, *CrystEngComm*, 2018, **20**, 3251–3257.

10 (*a*) L. Chen, P. S. Reiss, S. Y. Chong, D. Holden, K. E. Jelfs, T. Hasell, M. A. Little, A. Kewley, M. E. Briggs, A. Stephenson, K. M. Thomas, J. A. Armstrong, J. Bell, J. Busto, R. Noel, J. Liu, D. M. Strachan, P. K. Thallapally and A. I. Cooper, Separation of rare gases and chiral molecules by selective binding in porous organic cages, *Nat. Mater.*, 2014, **13**, 954–960; (*b*) M. Brutschy, M. W. Schneider, M. Mastalerz and S. R. Waldvogel, Porous organic cage compounds as highly potent affinity materials for sensing by quartz crystal microbalances, *Adv. Mater.*, 2012, **24**, 6049–6052; (*c*) X. Yang, J.-K. Sun, M. Kitta, H. Pang and Q. Xu, Encapsulating highly catalytically active metal nanoclusters inside porous organic cages, *Nat. Catal.*, 2018, **1**, 214–220; (*d*) T. Mitra, K. E. Jelfs, M. Schmidtmann, A. Ahmed, S. Y. Chong, D. J. Adams and A. I. Cooper, Molecular shape sorting using molecular organic cages, *Nat. Chem.*, 2013, **5**, 276–281.

11 (*a*) E. Martínez-Ahumada, D. He, V. Berryman, A. López-Olvera, M. Hernandez, V. Jancik, V. Martis, M. A. Vera, E. Lima, D. J. Parker, A. I. Cooper, I. A. Ibarra and M. Liu, SO_2 Capture Using Porous Organic Cages, *Angew. Chem. Int., Ed. Engl.*, 2021, **60**, 17556–17563; (*b*) T. Hasell, M. Schmidtmann and A. I. Cooper, Molecular doping of porous organic cages, *J. Am. Chem. Soc.*, 2011, **133**, 14920–14923.

12 (*a*) M. Liu, L. Zhang, M. A. Little, V. Kapil, M. Ceriotti, S. Yang, L. Ding, D. L. Holden, R. Balderas-Xicohténcatl, D. He, R. Clowes, S. Y. Chong, G. Schütz, L. Chen, M. Hirscher and A. I. Cooper, Barely porous organic cages for hydrogen isotope separation, *Science*, 2019, **366**, 613–

620; (*b*) M. Liu, M. A. Little, K. E. Jelfs, J. T. A. Jones, M. Schmidtmann, S. Y. Chong, T. Hasell and A. I. Cooper, Acid-and base-stable porous organic cages: shape persistence and pH stability via post-synthetic "tying" of a flexible amine cage, *J. Am. Chem. Soc.*, 2014, **136**, 7583–7586.

13 (*a*) T. Hasell, S. Y. Chong, K. E. Jelfs, D. J. Adams and A. I. Cooper, Porous organic cage nanocrystals by solution mixing, *J. Am. Chem. Soc.*, 2012, **134**, 588–598; (*b*) M. E. Briggs, A. G. Slater, N. Lunt, S. Jiang, M. A. Little, R. L. Greenaway, T. Hasell, C. Battilocchio, S. V. Ley and A. I. Cooper, Dynamic flow synthesis of porous organic cages, *Chem. Commun.*, 2015, **51**, 17390–17393; (*c*) J. Lucero, C. Osuna, J. M. Crawford and M. A. Carreon, Microwave-assisted synthesis of porous organic cages CC3 and CC2, *CrystEngComm*, 2019, **21**, 4534–4537; (*d*) B. D. Egleston, M. C. Brand, F. Greenwell, M. E. Briggs, S. L. James, A. I. Cooper, D. E. Crawford and R. L. Greenaway, Continuous and scalable synthesis of a porous organic cage by twin screw extrusion (TSE), *Chem. Sci.*, 2020, **11**, 6582–6589.

14 T. Tozawa, J. T. A. Jones, S. I. Swamy, S. Jiang, D. J. Adams, S. Shakespeare, R. Clowes, D. Bradshaw, T. Hasell, S. Y. Chong, C. Tang, S. Thompson, J. Parker, A. Trewin, J. Bacsa, A. M. Z. Slawin, A. Steiner and A. I. Cooper, Porous organic cages, *Nat. Mater.*, 2009, **8**, 973–978.

15 S.-L. Zheng, Y. He, X.-K. Qiu, Y.-H. Zhong, L.-H. Chung, W.-M. Liao and J. He, Synthesis, structures and Br_2 uptake of Cu(I)-bipyrazole frameworks, *J. Solid State Chem.*, 2021, **302**, 122458.

16 (*a*) H. Wang, A. Zhou, F. Peng, H. Yu and J. Yang, Mechanism study on adsorption of acidified multiwalled carbon nanotubes to Pb(II), *J. Colloid Interface Sci.*, 2007, **316**, 277–283; (*b*) Y. Liu, New insights to pseudo-second-order kinetic equation for adsorption, *Colloids Surf., A*, 2008, **320**, 275–278.

17 (*a*) K. Takai, H. Kumagai, H. Sato and T. Enoki, Bromine-adsorption-induced change in the electronic and magnetic properties of nanographite network systems, *Phys. Rev. B: Condens. Matter Mater. Phys.*, 2006, **73**, 035435; (*b*) H. Sato, N. Kawatsu, T. Enoki, M. Endo, R. Kobori, S. Maruyama and K. Kaneko, Drastic effect of water-adsorption on the magnetism of carbon nanomagnets, *Solid State Commun.*, 2003, **125**, 641–645.

18 (*a*) Q. Song, W. D. Wang, X. Hu and Z. Dong, Ru nanoclusters confined in porous organic cages for catalytic hydrolysis of ammonia borane and tandem hydrogenation reaction, *Nanoscale*, 2019, **11**, 21513–21521; (*b*) T. Gelles, A. A. Rownaghi and F. Rezaei, Diffusion Kinetics of CO_2, CH_4, and their Binary Mixtures in Porous Organic Cage CC3, *J. Phys. Chem. C*, 2019, **123**, 24172–24180.

19 (*a*) C. A. Coulson and G. N. Robertson, A Theory of the Broadening of the Infrared Absorption Spectra of Hydrogen-Bonded Species. II. The Coupling of Anharmonic ν (XH) and ν (XH.Y) Modes, *Proc. R. Soc. London Ser. A*, 1975, **342**, 289–315; (*b*) G. R. Satyanarayana, D. B. K. Kumar and K. Sujatha, Probing the intermolecular interactions in the binary liquid mixtures of o-chlorophenol with alkoxyethanols through ultrasonic, transport and FT-IR spectroscopic studies at different temperatures, *J. Mol. Liq.*, 2016, **216**, 526–537.

20 (*a*) L. G. Bulusheva, A. V. Okotrub, E. Flahaut, I. P. Asanov, P. N. Gevko, V. O. Koroteev, Y. V. Fedoseeva, A. Yaya and C. P. Ewels, Bromination of double-walled carbon nanotubes, *Chem. Mater.*, 2012, **24**, 2708–2715; (*b*) I. Mazov, D. Krasnikov, A. Stadnichenko, V. Kuznetsov, A. Romanenko, O. Anikeeva and E. Tkachev, Direct vapor-phase bromination of multiwall carbon nanotubes, *J. Nanotechnol.*, 2012, 954084; (*c*) E. Papirer, R. Lacroix and J.-B. Donnet, XPS Study of the halogenation of carbon black-part 1. Bromination, *Carbon*, 1994, **32**, 1341–1358.

21 H. S. O. Chan, H. S. Munro, C. Davies and E. T. Kang, XPS studies of chemically synthesized polypyrrole-halogen charge transfer complexes, *Synth. Met.*, 1988, **22**, 365–370.

22 (*a*) J. E. Cahill and G. E. Leroi, Raman spectra of solid chlorine and bromine, *J. Chem. Phys.*, 1969, **51**, 4514–4519; (*b*) E. T. Branigan, M. N. van Staveren and V. A. Apkarian, Solidlike coherent vibronic dynamics in a room temperature liquid: Resonant Raman and absorption spectroscopy of liquid bromine, *J. Chem. Phys.*, 2010, **132**, 044503; (*c*) K. P. Huber and G. Herzberg, Constants of Diatomic Molecules (data prepared by J.W. Gallagher, R.D. Johnson, III), in *NIST Chemistry WebBook, NIST Standard Reference Database Number 69*, ed. P. J. Linstrom and W. G. Mallard, National Institute of Standards and Technology, Gaithersburg MD, 2001, p. 20899, **https://webbook.nist.gov/**.

23 (*a*) A. L. Aguiar, E. B. Barros, V. P. Sousa Filho, H. Terrones, V. Meunier, D. Machon, Y. A. Kim, H. Muramatsu, M. Endo, F. Baudelet, A. San-Miguel and A. G. Souza Filho, Pressure tuning of bromine ionic states in double-walled carbon nanotubes, *J. Phys. Chem. C*, 2017, **121**, 10609–10619; (*b*) G. M. do Nascimento, T. Hou, Y. A. Kim, H. Muramatsu, T. Hayashi, M. Endo, N. Akuzawa and M. S. Dresselhaus, Double-Wall Carbon Nanotubes Doped with Different Br_2 Doping Levels: A Resonance Raman Study, *Nano Lett.*, 2008, **8**, 4168–4172; (*c*) J. C. Evans and G. Y. S. Lo, Vibrational spectra of BrO^-, BrO_2^-, Br_3^-, and Br_5, *Inorg. Chem.*, 1967, **6**, 1483–1486; (*d*) X. Chen, M. A. Rickard, J. W. Hull Jr, C. Zheng, A. Leugers and P. Simoncic, Raman spectroscopic investigation of tetraethylammonium polybromides, *Inorg. Chem.*, 2010, **49**, 8684–8689.

24 (*a*) O. V. Sedelnikova, C. P. Ewels, D. V. Pinakov, G. N. Chekhova, E. Flahaut, A. V. Okotrub and L. G. Bulusheva, Bromine polycondensation in pristine and fluorinated graphitic carbons, *Nanoscale*, 2019, **11**, 15298–15306; (*b*) A. Yaya, C. P. Ewels, J. K. Efavi, B. Agyei-Tuffour, K. Kan-Dapaah, B. Onwona-Agyeman, E. K. K. Abavare, A. Hassanali and P. R. Briddon, A study of polybromide chain formation using carbon nanomaterials via density functional theory approach, *Cogent Eng.*, 2016, **3**, 1261509.

25 Z. Ghalami, V. Ghoulipour and A. R. Khanchi, Adsorption and sequential thermal release of F_2, Cl_2, and Br_2 molecules by a porous organic cage material (CC3-R): Molecular dynamics and grand-canonical Monte Carlo simulations, *J. Comput. Chem.*, 2020, **41**, 949–957.

